

Enhanced the Complete Photonic Band Gaps for Three-Dimensional Photonic Crystals Consisting of Epsilon-Negative Materials in Pyrochlore Arrangement

Hai-Feng Zhang^{1, 2, *}, Shao-Bin Liu¹, and Hui-Chao Zhao^{1, 3}

Abstract—In this paper, the properties of photonic band gaps (PBGs) for three-dimensional (3D) photonic crystals (PCs) composed of isotropic positive-index materials and epsilon-negative materials with pyrochlore lattices are theoretically investigated by a modified plane wave expansion method. The eigenvalue equations of calculating the band structures for such 3D PCs in the first irreducible Brillouin zone (spheres with the isotropic positive-index materials inserted in the epsilon-negative materials background) are theoretically deduced. Numerical simulations show that the PBG and a flatbands region can be achieved. It is also found that larger PBG can be obtained in such PCs structure than the conventional lattices, such as diamond, face-centered-cubic, body-centered-cubic and simple-cubic lattices. The influences of the relative dielectric constant of spheres, filling factor, electronic plasma frequency, dielectric constant of epsilon-negative materials and damping factor on the properties of PBG for such 3D PCs are studied in detail, respectively, and some corresponding physical explanations are also given. The calculated results also show that the PBG can be manipulated by the parameters mentioned above except for the damping factor. Introducing the epsilon-negative materials into 3D dielectric PCs can obtain the complete and larger PBG as such 3D PCs with pyrochlore lattices, and also provides a way to design the potential devices.

1. INTRODUCTION

Since firstly proposed by Yablonovitch [1] and John [2], photonic crystals (PCs) have received ever-increasing interest during the past 20 years. The conventional PCs are artificial materials, in which different dielectrics are periodically arranged in spaces. PCs can produce special regions named photonic band gaps (PBGs) originating from the interface of Bragg scattering [3,4], which can control the propagation of electromagnetic wave (EM wave). This feature makes PCs potentially be used to design various applications due to their ability to control the propagation of light, such as defect cavities [5], waveguide [6], defect-mode PCs lasers [7], filter [8], omnidirectional reflector [9,10], and band-edge lasers [11–13]. However, the PBGs of conventional PCs will suffer from high sensitivity to the lattices and randomness, which means that PBGs cannot be changed as the dielectrics and topology of PCs are certain, and may also be affected by the errors in manufacturing. To overcome these drawbacks, researchers have to introduce metamaterials into the PCs to obtained tunable PBGs [14] and zero- \bar{n} PBGs [15]. Obviously, the zero-refractive indices can be obtained by metamaterials [16,17]. Metamaterials are firstly proposed by Veselago in 1967 [18], and can exhibit a negative index of refraction in some frequency ranges. Due to this, metamaterials can exhibit some unusual physical properties, such as inverse Snell's law, Cherenkov effects and reversed Doppler effects. Metamaterials can be divided into two categories. One is named double-negative metamaterials whose permittivity ε and permeability μ

Received 28 February 2014, Accepted 8 April 2014, Scheduled 25 April 2014

* Corresponding author: Hai Feng Zhang (hanlor@163.com).

¹ Key Laboratory of Radar Imaging and Microwave Photonics (Nanjing University of Aeronaut. Astronaut.), Ministry of Education, Nanjing University of Aeronautics and Astronautics, Nanjing 210016, China. ² Nanjing Artillery Academy, Nanjing 211132, China.

³ No. 96625 Troops of PLA, Zhangjiakou 075100, China.

are simultaneously negative [19], and the other is called single-negative metamaterials [20]. The single-negative metamaterials can also be divided into two types. One configuration, in which ε is negative, but μ is positive, gives rise to so-called epsilon-negative (ENG) materials. The other is that ε is positive, but μ is negative. In this case, mu-negative (MNG) materials can be obtained. It has been reported that stacking alternating layers of ENG materials and MNG materials can obtain zero- \bar{n} PBGs and zero-effective-phase PBGs [21]. Moreover, the double-negative metamaterials can hardly be found in nature, but ENG materials can always be found easily in the practical applications in different frequency regions, such as plasma [22–24], superconductors [25–27], semiconductors [28] and metals [29]. Compared to the conventional PCs, the PCs containing ENG materials display strong spatial dispersion [30]. Thus, the PCs containing ENG materials become a new research focus and have been extremely investigated. The most extensive works to date on such kind of PCs are reported on the one-dimensional (1D) or 2D structures. Such 1D and 2D PCs structures can be used to design the omnidirectional mirrors [31], omnidirectional filter [32], omnidirectional reflector [33], etc. However, the 1D and 2D PCs structures cannot be found in the real applications for the finite periodic structures, and 3D PCs structure may be closer to the actual situation. Compared to 1D and 2D cases, reports on 3D PCs with ENG materials are few. For example, the 3D PCs containing metals have been investigated in theory and experiment [34–36], and dispersive properties of 3D plasma PCs [37–39] have also been reported recently. From these research results, we can know that the topology of 3D PCs is a key to obtain complete PBGs. If 3D PCs contain ENG materials with high symmetry, such as face-centered-cubic (fcc) lattices [40], simple-cubic (sc) lattices [38], and body-centered-cubic (bcc) lattices [41], the complete PBGs can hardly be achieved, unless the dielectric constant of dielectric is sufficiently large so that the resonant scattering of EM waves is prominent enough to open a complete band gap [42, 43]. Unfortunately, technological difficulties can be found in fabricating such kind of high symmetry 3D PCs to achieve the complete PBGs with the large dielectric constant of dielectric. To solve these problems, some methods have been reported: the symmetry reduction [44], introducing anisotropy in dielectric [45], or fabricating in a new topology [46]. As reported by Garcia-Adeva [47, 48], the pyrochlore lattice is a good candidate to obtain complete PBGs for 3D PCs and can also be fabricated. Therefore, we can introduce ENG materials into 3D PCs with pyrochlore lattice to achieve the larger complete PBGs as the filling factor and the relative dielectric constant of filling dielectric are small.

The aims of this paper are to explore a better geometrical structure to obtain larger complete PBGs and investigate the properties of PBG for 3D PCs composed of isotropic positive-index materials and ENG materials with pyrochlore lattices, which are theoretically studied by a modified plane wave expansion (PWE) method. The more general model of ENG materials and damping factor are considered, and the periodic structures of PCs are infinite whose spheres with isotropic dielectric inserted in the ENG materials background periodically with pyrochlore lattices. This paper is organized as follows. The equations of computing the band structures for such 3D PCs are theoretically deduced in Section 2. In Section 3, the influences of the relative dielectric constant of spheres, filling factor, electronic plasma frequency, dielectric constant of ENG materials and damping factor on the properties of PBG for are investigated, respectively. Finally, conclusions are drawn in Section 4. An $e^{-j\omega t}$ time-dependence is implicit through the paper, with t the time, and $j = \sqrt{-1}$. We also consider c as light speed in vacuum.

2. THEORY AND NUMERICAL METHOD

The first irreducible Brillouin zone and schematic structure of 3D PCs containing ENG materials with a spherical atom in pyrochlore lattice can be found in Fig. 1. We assume that the dielectric and ENG materials are isotropic and homogeneous and that the relative dielectric functions are ε_a and ε_p , respectively. We denote the radius of the spheres and lattice constant are R and a , respectively. In the following numerical calculations, ENG material is assumed to be dispersive with effective dielectric function ε_p which can be written as [40]

$$\varepsilon_p(\omega) = \varepsilon_b - \frac{\omega_p^2}{\omega(\omega + j\gamma)} \quad (1)$$

where ε_b , ω_p and γ are the dielectric constant of ENG materials, the electronic plasma frequency and the damping factor that contributes to the absorption and losses, respectively. In order to obtain the PBGs

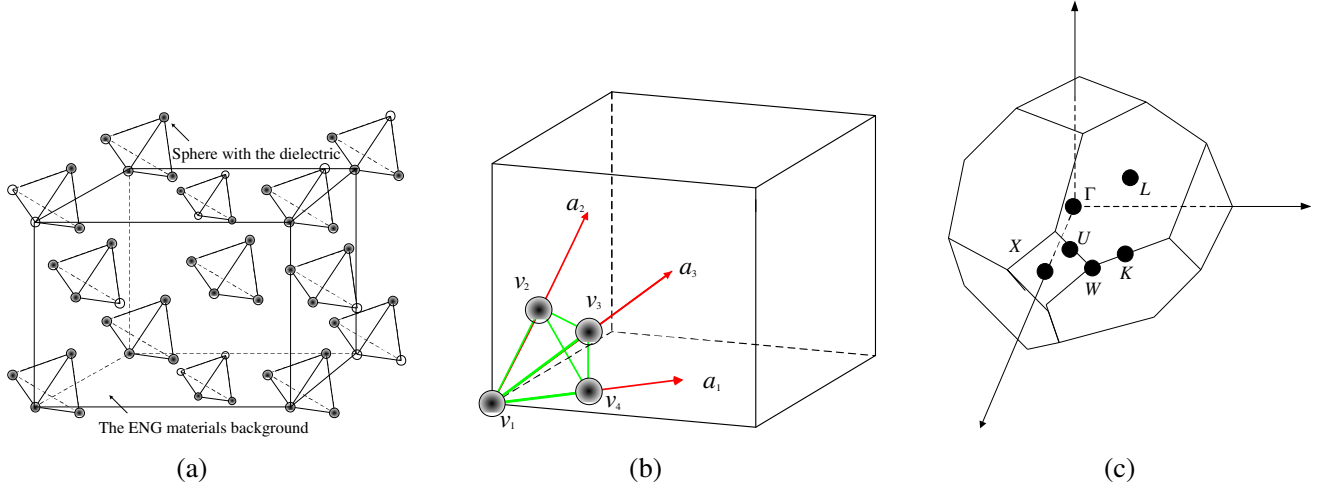


Figure 1. Schematic structure of such 3D PCs with pyrochlore lattices. (a) 3D PCs structure, (b) rhombohedral axes with respect to the cubic unit cell, and (c) the first irreducible Brillouin zone showing symmetry point used for computing the anisotropic PBGs, respectively.

of such 3D PCs, several efficient numerical methods have been reported [49–51]. Among these methods, the PWE method is the most popular one to achieve the band structures. Especially, Zhang et al. [52], and Kuzmiak and Maradudin [53] proposed a modified PWE method, which can successfully calculate PBGs for the PCs composed of Drude-type medium. As mentioned in [52], a standard linearization technique was used to solve the general nonlinear eigenvalue equation. Thus, the PCs composed of ENG material can be calculated easily by such a method. In this paper, the same technique will also be used to calculate the PBGs of such 3D PCs. As we know, the Maxwell’s equation for magnetic field in such 3D PCs can be expressed as:

$$\nabla \times \left[\frac{1}{\varepsilon(\mathbf{r})} \nabla \times \mathbf{H} \right] = \frac{\omega^2}{c^2} \mathbf{H} \tag{2}$$

Since $\varepsilon(\mathbf{r})$ is periodic, we can use Bloch’s theorem to expand the \mathbf{H} field in term of plane wave,

$$\mathbf{H}(\mathbf{r}) = \sum_{\mathbf{G}} \sum_{\lambda=1}^2 h_{\mathbf{G},\lambda} \widehat{\mathbf{e}}_{\lambda} e^{j(\mathbf{k}+\mathbf{G})\cdot\mathbf{r}} \tag{3}$$

where \mathbf{k} is a wave vector in the Brillouin zone of lattice, \mathbf{G} a reciprocal-lattice vector, and $\widehat{\mathbf{e}}_1, \widehat{\mathbf{e}}_2$ are orthogonal unit vectors that are both perpendicular to wave vector $\mathbf{k} + \mathbf{G}$ because of the transverse character of magnetic field \mathbf{H} (i.e., $\nabla \cdot \mathbf{H} = 0$). The 3D Bravais lattice is spanned by three primitive vectors $\mathbf{a}_1, \mathbf{a}_2$ and \mathbf{a}_3 , respectively. The dielectric structure satisfies the boundary conditions

$$\varepsilon(\mathbf{r} + \mathbf{a}_i) = \varepsilon(\mathbf{r}) \tag{4}$$

The reciprocal lattice vectors $\mathbf{b}_1, \mathbf{b}_2$ and \mathbf{b}_3 are defined by

$$\mathbf{a}_i \cdot \mathbf{b}_j = 2\pi\delta_{ij} \tag{5}$$

where δ_{ij} is the Kronecker delta symbol. The dielectric constant dyadic can also be expanded into its Fourier form as

$$\varepsilon^{-1}(\mathbf{r}) = \varepsilon_{\mathbf{G},\mathbf{G}'}^{-1} = \sum_{\mathbf{G}} \eta(\mathbf{G}) e^{j\mathbf{G}\cdot\mathbf{r}} \tag{6}$$

where $\eta(\mathbf{G})$ is the Fourier transform of the inverse of $\varepsilon(\mathbf{r})$, and the sum is taken over every reciprocal lattice vector \mathbf{G} , which is a linear combination of $\mathbf{b}_1, \mathbf{b}_2$ and \mathbf{b}_3 :

$$\mathbf{G} = l_1\mathbf{b}_1 + l_2\mathbf{b}_2 + l_3\mathbf{b}_3 \tag{7}$$

where l_1 , l_2 and l_3 are integers. The Fourier coefficient is expressed by

$$\eta(\mathbf{G}) = \frac{1}{S_1} \int_{s_1} d\mathbf{r} \frac{1}{\varepsilon(\mathbf{r})} e^{-j\mathbf{G}\cdot\mathbf{r}} \quad (8)$$

where S_1 denotes the area of the unit cell. For a given lattice with a unit cell including n_s scatters, $\eta(\mathbf{G})$ is given by [54]:

$$\eta(\mathbf{G}) = \varepsilon_a^{-1} \delta_{\mathbf{G},0} + \sum_{i=1}^{n_s} \eta^{(i)}(\mathbf{G}) e^{-j\mathbf{G}\cdot\mathbf{r}_i} \quad (9)$$

and $\eta^{(i)}(\mathbf{G})$ is the Fourier transform of each scatter of lattice unit cell at position \mathbf{r}_i . n_s is the number of scatters in a unit cell with pyrochlore lattices. It is worth noting that the pyrochlore lattice (see Fig. 1(a)) has a rhombohedral primitive unit cell with lattice vectors,

$$\mathbf{a}_1 = (0.5, 0.5, 0), \quad \mathbf{a}_2 = (0.5, 0, 0.5), \quad \mathbf{a}_3 = (0, 0.5, 0.5),$$

with a four-atom basis at positions, $\mathbf{v}_1 = (0, 0, 0)$, $\mathbf{v}_2 = \mathbf{a}_2/2$, $\mathbf{v}_3 = \mathbf{a}_3/2$, $\mathbf{v}_4 = \mathbf{a}_1/2$, as shown in Fig. 1(b). Substituting Eq. (3) and Eq. (6) into Eq. (2), the following linear matrix equations can be obtained

$$\sum_{\mathbf{G}', \lambda'} H_{\mathbf{G}, \mathbf{G}'}^{\lambda, \lambda'} h_{\mathbf{G}', \lambda'} = \frac{\omega^2}{c^2} h_{\mathbf{G}, \lambda} \quad (10)$$

where

$$H_{\mathbf{G}, \mathbf{G}'}^{\lambda, \lambda'} = |\mathbf{k} + \mathbf{G}| |\mathbf{k} + \mathbf{G}'| \begin{pmatrix} \hat{\mathbf{e}}_2 \cdot \varepsilon_{\mathbf{G}, \mathbf{G}'}^{-1} \cdot \hat{\mathbf{e}}_2' & -\hat{\mathbf{e}}_2 \cdot \varepsilon_{\mathbf{G}, \mathbf{G}'}^{-1} \cdot \hat{\mathbf{e}}_1' \\ -\hat{\mathbf{e}}_1 \cdot \varepsilon_{\mathbf{G}, \mathbf{G}'}^{-1} \cdot \hat{\mathbf{e}}_2' & \hat{\mathbf{e}}_1 \cdot \varepsilon_{\mathbf{G}, \mathbf{G}'}^{-1} \cdot \hat{\mathbf{e}}_1' \end{pmatrix} \quad (11)$$

where $\varepsilon_{\mathbf{G}, \mathbf{G}'}^{-1} = \eta(\mathbf{G} - \mathbf{G}')$. In order to solve Eq. (11), we use the expansion of Eq. (4), and write $h_{\mathbf{G}, \lambda}$ in the form

$$h_{\mathbf{G}, \lambda} = \sum_{\mathbf{G}} A(\mathbf{k}|\mathbf{G}) e^{j(\mathbf{k}+\mathbf{G})\cdot\mathbf{r}} \quad (12)$$

Assume that $f = (4\pi R^3)/(3V_m)$ is the filling factor of one sphere with the isotropic dielectric and V_m the volume of unit cell. The Fourier coefficients $\eta_{\mathbf{G}}$ can be written as [38–41]:

$$\eta_{\mathbf{G}} = \begin{cases} \left(\frac{\omega^2 + j\gamma\omega}{\varepsilon_b\omega^2 + j\varepsilon_b\gamma\omega - \omega_p^2} \right) 4f + \left(\frac{1}{\varepsilon_a} \right) (1 - 4f), & \mathbf{G} = 0 \\ \left(\left(\frac{\omega^2 + j\gamma\omega}{\varepsilon_b\omega^2 + j\varepsilon_b\gamma\omega - \omega_p^2} \right) - \frac{1}{\varepsilon_a} \right) \cdot \sum_{i=1}^4 e^{-j(\mathbf{G}\cdot\mathbf{v}_i)} \cdot 3f \left(\frac{\sin(|\mathbf{G}|R) - (|\mathbf{G}|R) \cos(|\mathbf{G}|R)}{(|\mathbf{G}|R)^3} \right), & \mathbf{G} \neq 0 \end{cases} \quad (13)$$

We can obtain the equation for the coefficients $\{A(\mathbf{k}|\mathbf{G})\}$

$$\begin{aligned} & \left(\frac{\omega^2 + j\gamma\omega}{\varepsilon_b\omega^2 + j\varepsilon_b\gamma\omega - \omega_p^2} \right) 4f + \left(\frac{1}{\varepsilon_a} \right) (1 - 4f) \cdot |\mathbf{k} + \mathbf{G}| |\mathbf{k} + \mathbf{G}'| \cdot \vec{\mathbf{F}} \cdot A(\mathbf{k}|\mathbf{G}) \\ & + \sum_{\mathbf{G}'} \left(\left(\frac{\omega^2 + j\gamma\omega}{\varepsilon_b\omega^2 + j\varepsilon_b\gamma\omega - \omega_p^2} \right) - \frac{1}{\varepsilon_a} \right) \cdot \sum_{i=1}^4 e^{-j(\mathbf{G}\cdot\mathbf{v}_i)} \cdot 3f \left(\frac{\sin(|\mathbf{G}|R) - (|\mathbf{G}|R) \cos(|\mathbf{G}|R)}{(|\mathbf{G}|R)^3} \right) \\ & \cdot |\mathbf{k} + \mathbf{G}| |\mathbf{k} + \mathbf{G}'| \cdot \vec{\mathbf{F}} \cdot A(\mathbf{k}|\mathbf{G}) = \frac{\omega^2}{c^2} A(\mathbf{k}|\mathbf{G}) \end{aligned} \quad (14)$$

where the prime on the sum over \mathbf{G}' indicates that the term with $\mathbf{G}' = \mathbf{G}$ is omitted. We consider

$\vec{\mathbf{F}} = \begin{pmatrix} \hat{\mathbf{e}}_2 \cdot \hat{\mathbf{e}}_2' & -\hat{\mathbf{e}}_2 \cdot \hat{\mathbf{e}}_1' \\ -\hat{\mathbf{e}}_1 \cdot \hat{\mathbf{e}}_2' & \hat{\mathbf{e}}_1 \cdot \hat{\mathbf{e}}_1' \end{pmatrix}$. At this point we use the definition of a complex variable μ given by

$$\mu = \omega/c \quad (15)$$

Eq. (13) yields

$$\mu^4 \vec{\mathbf{I}} - \mu^3 \vec{\mathbf{T}} - \mu^2 \vec{\mathbf{U}} - \mu \vec{\mathbf{V}} - \vec{\mathbf{W}} = 0 \quad (16)$$

$$\vec{\mathbf{T}}(\mathbf{G}|\mathbf{G}') = -j\frac{\gamma}{c}\delta_{\mathbf{G},\mathbf{G}'}, \quad (17a)$$

$$\vec{\mathbf{U}}(\mathbf{G}|\mathbf{G}') = \left\{ \frac{\omega_p^2}{\varepsilon_b^2 c^2} + \left(\frac{1}{\varepsilon_a} 4f + \frac{(1-4f)}{\varepsilon_b} \right) \cdot |\mathbf{k} + \mathbf{G}| |\mathbf{k} + \mathbf{G}'| \cdot \vec{\mathbf{F}} \right\} \delta_{\mathbf{G},\mathbf{G}'} + \left(\frac{1}{\varepsilon_a} - \frac{1}{\varepsilon_b} \right) \vec{\mathbf{M}} \quad (17b)$$

$$\vec{\mathbf{V}}(\mathbf{G}|\mathbf{G}') = \left\{ \left(j\frac{\gamma}{c} \left(\frac{1}{\varepsilon_a} 4f + \frac{(1-4f)}{\varepsilon_b} \right) \right) \cdot |\mathbf{k} + \mathbf{G}| |\mathbf{k} + \mathbf{G}'| \cdot \vec{\mathbf{F}} \right\} \delta_{\mathbf{G},\mathbf{G}'} + j\frac{\gamma}{c} \left(\frac{1}{\varepsilon_a} - \frac{1}{\varepsilon_b} \right) \vec{\mathbf{M}} \quad (17c)$$

$$\vec{\mathbf{W}}(\mathbf{G}|\mathbf{G}') = \left\{ -\frac{\omega_p^2}{c^2} \frac{1}{\varepsilon_b \varepsilon_a} (1-f) \cdot |\mathbf{k} + \mathbf{G}| |\mathbf{k} + \mathbf{G}'| \cdot \vec{\mathbf{F}} \right\} \delta_{\mathbf{G},\mathbf{G}'} + \frac{\omega_p^2}{c^2} \left(\frac{1}{\varepsilon_b^2} - \frac{1}{\varepsilon_b \varepsilon_a} \right) \vec{\mathbf{M}} \quad (17d)$$

where $\vec{\mathbf{M}} = |\mathbf{k} + \mathbf{G}| |\mathbf{k} + \mathbf{G}'| \cdot \vec{\mathbf{F}} \cdot \sum_{i=1}^4 e^{-(\mathbf{G} \cdot \mathbf{v}_i)} \cdot 3f \left(\frac{\sin(|\mathbf{G}|R) - (|\mathbf{G}|R) \cos(|\mathbf{G}|R)}{(|\mathbf{G}|R)^3} \right)$, the element of the $N \times N$ matrices are, $\vec{\mathbf{T}}$, $\vec{\mathbf{U}}$, $\vec{\mathbf{V}}$ and $\vec{\mathbf{W}}$. This polynomial form can be transformed into a linear problem in $4N$ dimension by $\vec{\mathbf{Q}}$ that fulfills

$$\vec{\mathbf{Q}}z = \mu z, \quad \vec{\mathbf{Q}} = \begin{bmatrix} \mathbf{0} & \vec{\mathbf{I}} & \mathbf{0} & \mathbf{0} \\ \mathbf{0} & \mathbf{0} & \vec{\mathbf{I}} & \mathbf{0} \\ \mathbf{0} & \mathbf{0} & \mathbf{0} & \vec{\mathbf{I}} \\ \vec{\mathbf{W}} & \vec{\mathbf{V}} & \vec{\mathbf{U}} & \vec{\mathbf{T}} \end{bmatrix} \quad (18)$$

The complete solution of Eq. (16) is obtained by computing the eigenvalues of Eq. (18). Of course the dispersion relation can be determined by the real part of such eigenvalues.

3. RESULTS AND DISCUSSION

In order to investigate the PBGs properties of 3D PCs with pyrochlore lattices composed of ENG materials, the band structures are calculated in the first irreducible Brillouin zone as shown in Fig. 1(c). As we know [46–48], the high symmetry points have the coordinate as $\Gamma = (0, 0, 0)$, $X = (2\pi/a, 0, 0)$, $W = (2\pi/a, \pi/a, 0)$, $K = (1.5\pi/a, 1.5\pi/a, 0)$, $L = (\pi/a, \pi/a, \pi/a)$, and $U = (2\pi/a, 0.5\pi/a, 0.5\pi/a)$. The convergence accuracy is better than 1% for the lower energy bands as a total number of 1331 plane waves can be used [38–41]. Without loss of generality, we plot $\omega a/2\pi c$ with the normalization convention $\omega_{p0} a/2\pi c = 1$. With this definition, we can let a take any value as long as R is shifted according to achieve the same filling factors. Thus, we can define the electronic plasma frequency as $\omega_p = \omega_{pl} = 0.05\omega_{p0}$ to make the problem scale-invariant, and we also choose the damping factor as $\gamma = 0.02\omega_{pl}$, $\mu_a = 1$, and $\mu_p = 1$, respectively. Here, we only focus on the properties of first (1st) PBG for such 3D PCs. In order to investigate the PBG properties of such 3D PCs, the relative bandwidth of PBG is defined as

$$\Delta\omega/\omega_i = 2(\omega_1 - \omega_2) / (\omega_1 + \omega_2) \quad (19)$$

where ω_1 and ω_2 are the upper and lower limits of a PBG, respectively.

Firstly, we consider a simple case and assume $\varepsilon_b = 1$. In Fig. 2, we display the dispersive curves for 3D PCs with pyrochlore lattices containing ENG materials as $\varepsilon_b = 1$, $\omega_p = 0.15\omega_{p0}$, $\gamma = 0.02\omega_{pl}$ and $R = 0.19a$ but with different the electronic plasma frequency of the ENG material. The red-shaded regions indicate the PBGs. As shown in Fig. 2(a), if $\omega_p = 0$, the ENG materials can be looked as the air, and such 3D PCs become dielectric-air PCs. There is a PBG in the frequency region $0-2\pi c/a$, which presents itself at $0.3911-0.4510$ ($2\pi c/a$). As ENG material is introduced into such 3D PCs, the band diagram for $\omega_p = 0.05\omega_{p0}$ is also plotted in Fig. 2(b). It can be seen from Fig. 2(b) that one PBG and one flatbands region can be found. The PBG covers $0.3922-0.4526$ ($2\pi c/a$), and the region of flatbands runs from 0 to 0.05 ($2\pi c/a$). There exists the flatbands region because of the existence of surface plasmon modes, and the plasmon resonance bands are around the cutoff frequencies of the ENG materials [40]. If the frequency of EM wave is located in the flatbands region, the real part of dielectric function of ENG material is negative. However, the real part of dielectric function of dielectric sphere is positive. Therefore, the surface plasmons can be found [55]. As we know, surface plasmons are waves

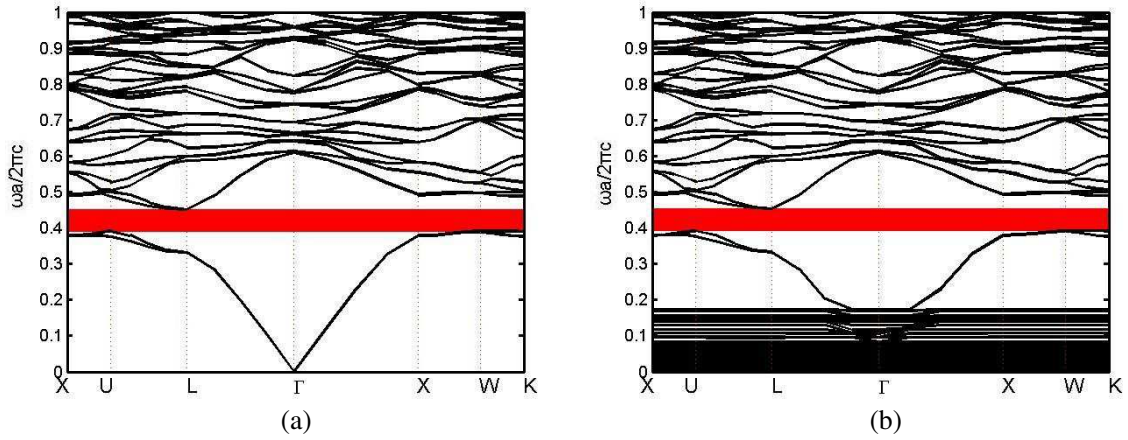


Figure 2. Calculated band structures for 3D PCs with pyrochlore lattices containing the ENG materials as $\varepsilon_b = 1$, $\varepsilon_a = 12$, $\gamma = 0.02\omega_{pl}$ and $R = 0.19a$ but with different the electronic plasma frequency. (a) $\omega_p = 0$; (b) $\omega_p = 0.05\omega_{p0}$, respectively.

that propagate along the surface of a conductor, due to collective oscillation of electric charges coupled with the electromagnetic field. Under suitable condition, surface plasmons may appear at interface across which the dielectric changes sign [55]. On the other hand, we consider a 3D case. The PBG for such 3D PCs is a complete PBG (for TE and TM modes). This can be seen in Eq. (11). Thus, for our case, the presence of the interface gives the field a longitudinal component due to discontinuity of the dielectric function across the interface. The motions of the electrons and EM fields can be coupled at the interface between the ENG materials and dielectric. However, because the fields inside the ENG materials have no longitudinal components to couple with the plasma oscillations, they rapidly decay away from interface. The surface plasmons are highly localized at the interface and evanescent otherwise [55]. If frequency of EM wave is located in the flatbands region, surface plasma waves, which are surface plasmon polaritons in the notation of 3D MPPCs, are present with very localized field around a dielectric sphere. Thus, the flatbands can be obtained. Compared to Fig. 2(a), the edges of PBG are upward to higher frequency region, and the bandwidth of PBG is increased by $0.0005(2\pi c/a)$. Thus, the PBG of 3D dielectric PCs can be enlarged by introducing the ENG materials. As we know, the 3D PCs containing the ENG materials with simpler lattices including the diamond, fcc, bcc and sc lattices can also produce the PBGs. As a comparison, we plot the photonic band structures of 3D PCs containing the ENG materials in various lattices as $\varepsilon_b = 1$, $\varepsilon_a = 12$, $\omega_p = 0.05\omega_{p0}$, $\gamma = 0.02\omega_{pl}$ and $R = 0.19a$ in Fig. 3. As we know, the high-symmetry points in the Brillouin zone for fcc and diamond lattices are the same as in the pyrochlore structure [46–48]. For the bcc lattices, the high-symmetry points are $\Gamma = (0, 0, 0)$, $H = (0, 0, 2\pi/a)$, $N = (0, \pi/a, \pi/a)$ and $P = (\pi/a, \pi/a, \pi/a)$. For the sc lattices, the high-symmetry points are $\Gamma = (0, 0, 0)$, $X = (\pi/a, 0, 0)$, $M = (\pi/a, \pi/a, 0)$, and $R = (\pi/a, \pi/a, \pi/a)$. It is clearly seen that the complete PBGs cannot be found in Figs. 3(a) and (d) due to band degeneracy at some high-symmetry points, which are H and P points for a bcc lattice, and M and R points for a sc lattice. This can be explained by the high symmetry of those lattices, and the dielectric constant of immersed dielectric sphere is not large enough to open a band gap [41]. It can also be seen from Figs. 3(b) and (c) that there are the PBGs of 3D PCs with fcc and diamond lattices, the 1st PBGs span $0.8131\text{--}0.8161(2\pi c/a)$ and $0.5956\text{--}0.6106(2\pi c/a)$, respectively. Obviously, the 3D PCs with pyrochlore lattices containing the ENG materials have a larger bandwidth of PBG than these PCs with the conventional simpler lattices, such as the diamond, fcc, sc and bcc structures. As mentioned above, the ENG materials introduced into the 3D dielectric PCs can enlarge the frequency range of PBG, and the larger PBG can be obtained as the 3D PCs with pyrochlore lattices.

In Fig. 4(a), we plot the dependences of the properties of 1st PBG for such 3D PCs on the filling factor of spheres as $\varepsilon_b = 1$, $\varepsilon_a = 12$, $\omega_p = 0.05\omega_{p0}$ and $\gamma = 0.02\omega_{pl}$, respectively. The shaded region indicates the PBG. Fig. 4(a) reveals that the edges of 1st PBG are downward to lower frequency region,

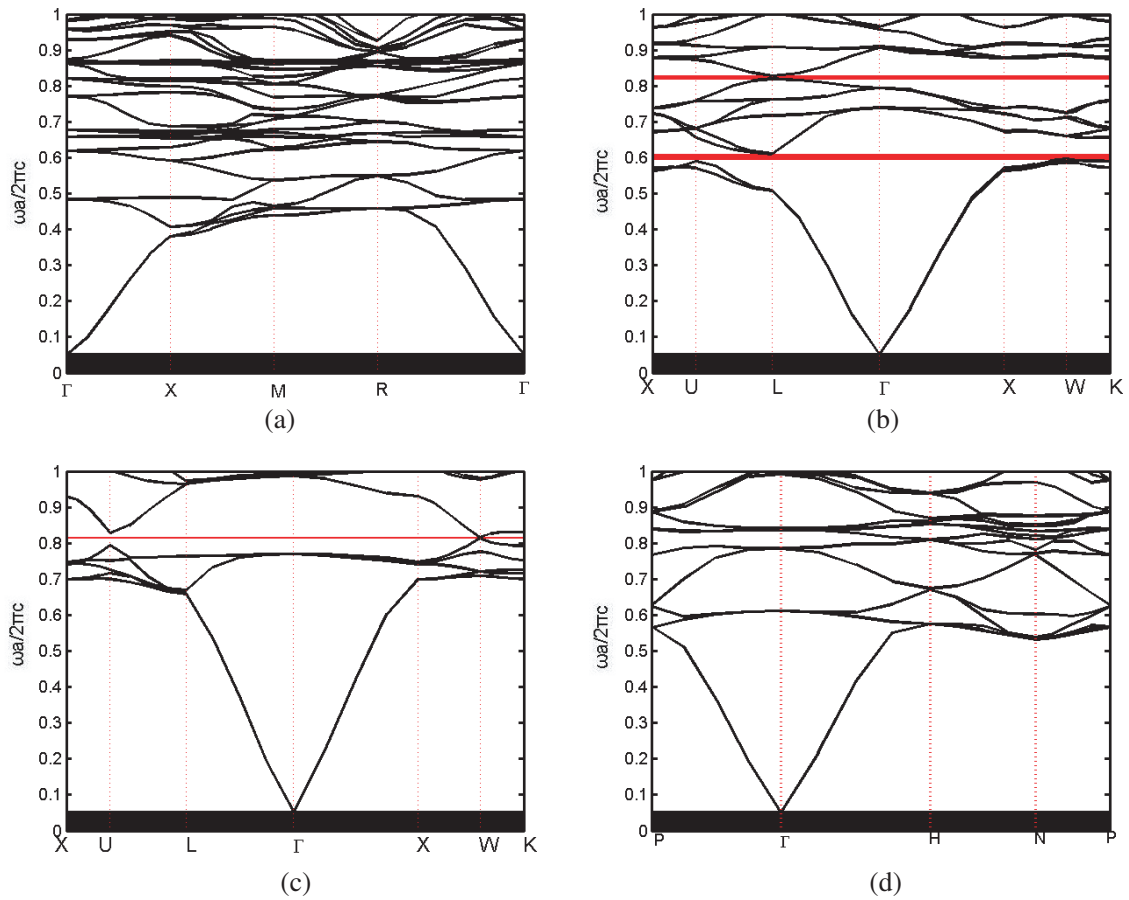


Figure 3. Calculated band structures for 3D PCs with four different conventional lattices containing the ENG materials as $\epsilon_b = 1$, $\epsilon_a = 12$, $\omega_p = 0.05\omega_{p0}$, $\gamma = 0.02\omega_{pl}$ and $R = 0.19a$. (a) sc lattices, (b) diamond lattices, (c) fcc lattices, and (d) bcc lattices, respectively.

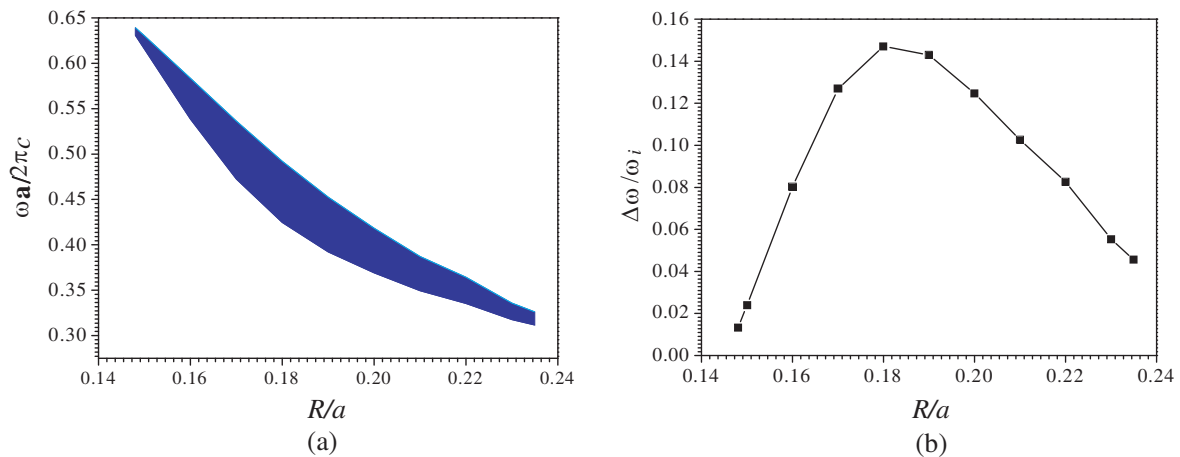


Figure 4. The effects of the radius of the dielectric spheres R/a on the PBG and relative bandwidth for such 3D PCs with $\epsilon_b = 1$, $\epsilon_a = 12$, $\omega_p = 0.05\omega_{p0}$ and $\gamma = 0.02\omega_{pl}$, respectively. The shaded region indicates the PBG. (a) The PBG, and (b) relative bandwidth.

and the bandwidth of 1st PBG increases first and then decreases with increasing the value of R/a . If the value of R/a is less than 0.148, there does not exist the 1st PBG, and it will disappear as the value of R/a is larger than 0.235. As R/a is increased from 0.05 to 0.48, the maximum bandwidth of 1st PBG is $0.0674 (2\pi c/a)$, which can be found in the case of $R/a = 0.18$. Compared to the case of $R/a = 0.19$, the maximum frequency range of 1st PBG is increased by $0.007 (2\pi c/a)$. Thus, the 1st PBG can be tuned by the filling factor of dielectric sphere. This can also be explained in physics that increasing the radius of the dielectric spheres means the space averaged dielectric constant of such 3D PCs becomes larger, and the PBG can be manipulated [38–41]. In Fig. 4(b), we plot the relative bandwidth ($\Delta\omega/\Delta\omega_i$) as a function of R/a . Fig. 4(b) shows that the relative bandwidth of 1st PBG increases first and then decreases with increasing the value of R/a . The maximum relative bandwidth of 1st PBG is 0.147, which can be found in the case of $R/a = 0.18$. Compared to the case of $R/a = 0.15$, the relative bandwidth of such a PBG is increased by 0.124. As mentioned above, the filling factor of dielectric spheres is an important parameter which needs to be chosen. It is also noticed that if the radius of the dielectric spheres is small enough and close to null, such 3D PCs can be looked as an ENG material block. The flatbands will disappear.

In Fig. 5(a), we plot the 1st PBG for such 3D PCs as a function of the relative dielectric constant of spheres ε_a . The parameters of 3D PCs are $\varepsilon_b = 1$, $\omega_p = 0.05\omega_{p0}$, $\gamma = 0.02\omega_{pl}$ and $R = 0.19a$. The shaded region indicates the PBG. As show in Fig. 5(a), the edges of 1st PBG for such 3D PCs shift to lower frequency region, and the bandwidth increases first and then decreases with increasing ε_a . If ε_a is less than 5, the 1st PBG will never appear. As ε_a is increased from 5 to 50, the 1st PBG runs from 0.1983 to $0.246 (2\pi c/a)$, and the bandwidth is $0.0477 (2\pi c/a)$. The frequency range is increased by $0.0184 (2\pi c/a)$ compared to the case of $\varepsilon_a = 5$. In Fig. 5(b), the relative bandwidth of 1st PBG is plotted. Fig. 5(b) illustrates that the general trend for 1st PBG is relative bandwidth which increases with increasing ε_a , and the maximum relative bandwidth is 0.215, which can be found in the case of $\varepsilon_a = 50$. This can be explained by that the bandwidths of PBGs are governed by refractive contrast for the dielectrics which compose such 3D PCs, and the positions of the PBGs are governed by the average refractive index of such 3D PCs [38–41]. As mentioned above, the frequency range of 1st PBG for such 3D PCs can be tuned by ε_a . The central frequency of 1st PBG shifts to lower frequency region, and the frequency bandwidth can be enlarged with increasing ε_a .

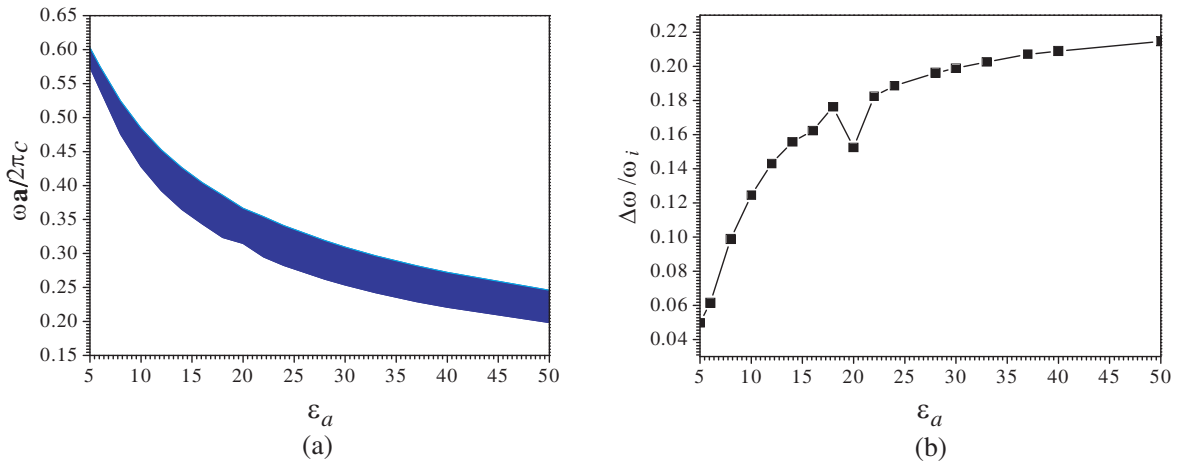


Figure 5. The effects of relative dielectric constant ε_a on the 1st PBG and relative bandwidth for such 3D PCs with $\varepsilon_b = 1$, $\omega_p = 0.05\omega_{p0}$, $\gamma = 0.02\omega_{pl}$ and $R = 0.19a$, respectively. The shaded region indicates the PBG. (a) The PBG, and (b) relative bandwidth.

In Fig. 6(a), we plot the effects of the electronic plasma frequency ω_p on the 1st PBG for such 3D PCs with $\varepsilon_b = 1$, $\varepsilon_a = 12$, $\gamma = 0.02\omega_{pl}$ and $R = 0.19a$, respectively. The shaded region indicates the PBG. As shown in Fig. 6(a), the edges of 1st PBG shift to higher frequency region with increasing the value of ω_p/ω_{p0} . The bandwidth of 1st PBG increases first and then decreases as the value of ω_p/ω_{p0} is

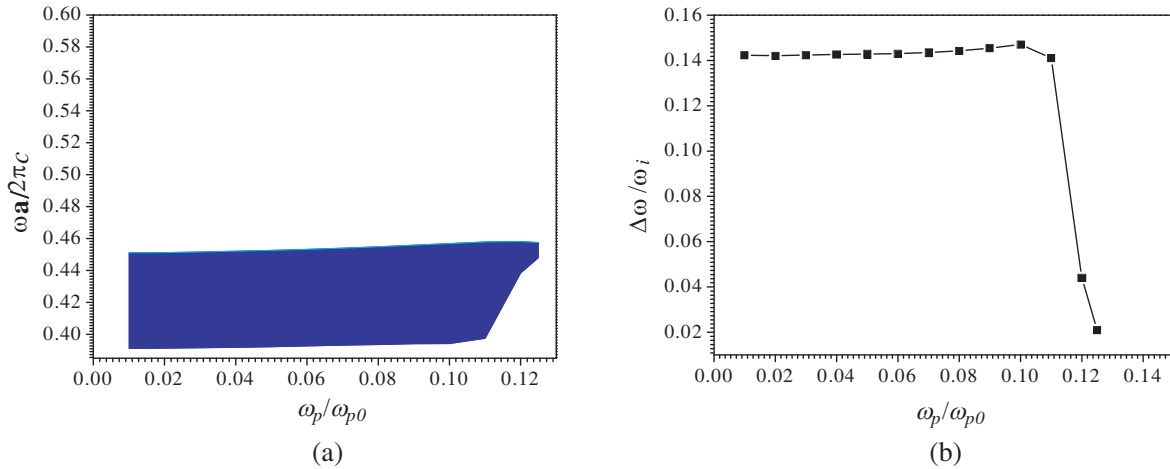


Figure 6. The effects of electronic plasma frequency ω_p on the 1st PBG and relative bandwidth for such 3D PCs with $\varepsilon_b = 1$, $\varepsilon_a = 12$, $\gamma = 0.02\omega_{pl}$ and $R = 0.19a$, respectively. The shaded region indicates the PBG. (a) The PBG, and (b) relative bandwidth.

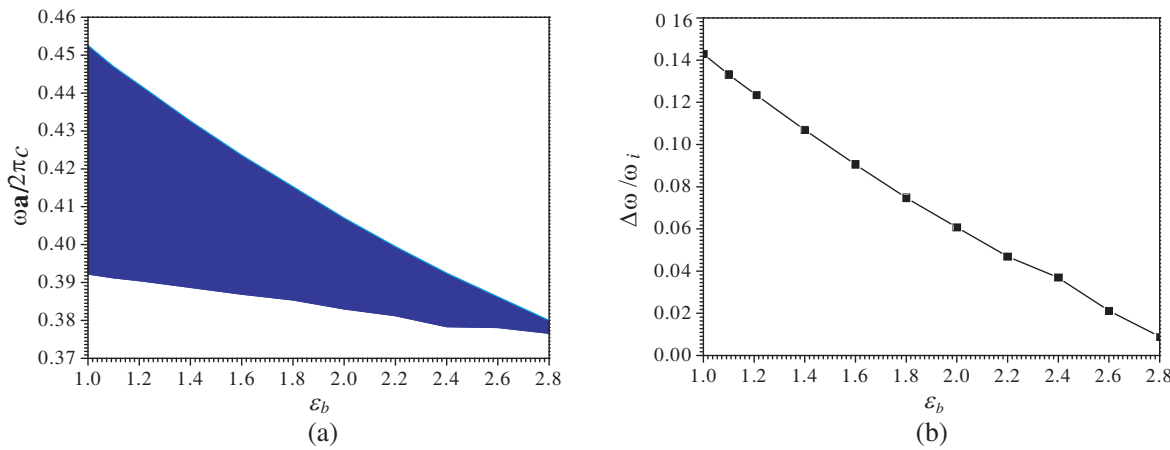


Figure 7. The effects of dielectric constant of ENG material ε_b on the 1st PBG and relative bandwidth for such 3D PCs with $\varepsilon_a = 12$, $\omega_p = 0.05\omega_{p0}$, $\gamma = 0.02\omega_{pl}$ and $R = 0.19a$, respectively. The shaded region indicates the PBGs. (a) The PBG, and (b) relative bandwidth.

increased. The 1st PBG will disappear as value of ω_p / ω_{p0} is larger than 0.125. As the value of ω_p / ω_{p0} is increased from 0.01 to 0.125, the 1st PBG is located from 0.448 to 0.4575 ($2\pi c/a$), and frequency range is 0.0049 ($2\pi c/a$). Compared to the case of $\omega_p / \omega_{p0} = 0.05$, the bandwidth of 1st PBG is decreased by 0.0504 ($2\pi c/a$). The maximum frequency range of 1st PBG is 0.0626 ($2\pi c/a$), which can be found in the case of $\omega_p / \omega_{p0} = 0.1$. In Fig. 6(b), the relative bandwidth as a function of electronic plasma frequency for 1st PBG is plotted. Fig. 6(b) shows that the relative bandwidth of 1st PBG increases first and then decreases as the value of ω_p / ω_{p0} is increased from 0.01 to 0.125. The maximum relative bandwidth is 0.14712, which can be found in the case of $\omega_p / \omega_{p0} = 0.1$. Compared to the case of $\omega_p / \omega_{p0} = 0.05$, the maximum relative bandwidth of 1st PBG is increased by 0.005. As mentioned above, PBG can be tuned by the electronic plasma frequency. This can be explained by that the average refractive index of such 3D PCs has been changed.

In Fig. 7(a), we plot the 1st PBG of such 3D PCs as a function of the dielectric constant of ENG materials ε_b with $\varepsilon_a = 12$, $\omega_p = 0.05\omega_{p0}$, $\gamma = 0.02\omega_{pl}$ and $R = 0.19a$, respectively. The shaded region indicates the PBGs. One can see from Fig. 7(a) that the edges of 1st PBG are linearly downward to

lower frequency region, and the bandwidth decreases with increasing ε_b . As ε_b is increased from 1 to 2.8, the 1st PBG presents itself at $0.3766\text{--}0.38 (2\pi c/a)$. Compared to the case of $\varepsilon_b = 1$, the bandwidth for 1st PBG is decreased by $0.057 (2\pi c/a)$. The maximum frequency range of 1st PBG can be found in the case $\varepsilon_b = 1$. In Fig. 7(b), the relative bandwidth of 1st PBG is also plotted. As shown in Fig. 7(b), the general trend for 1st PBG is that relative bandwidth decreases linearly with increasing ε_b . The maximum relative bandwidths for such PBG is 0.143, which can be found in the case of $\varepsilon_b = 1$. Compared to the case of $\varepsilon_b = 2.8$, the relative bandwidth is increased by 0.134. Similar to changing ε_a and ω_p , the way to change the dielectric constant of ENG material means that the refractive contrast for the dielectrics which compose such 3D PCs, and average refractive index of such 3D PCs are changed. Therefore, the PBG for such 3D PCs can be tuned by ε_b .

In Fig. 8(a), we plot the effects of damping factor γ on the 1st PBG for such 3D PCs with $\varepsilon_b = 1$, $\varepsilon_a = 12$, $\omega_p = 0.05\omega_{p0}$ and $R = 0.19a$, respectively. The shaded region indicates the PBG. As shown in Fig. 8(a), the 1st PBG for such 3D PCs can hardly be tuned by the damping factor of ENG materials. The frequency range of 1st PBG remains invariant, and the central frequencies also cannot be tuned with increasing the value of γ/ω_{pl} . The bandwidth of such PBGs runs from 0.3922 to 0.4526, as the value of γ/ω_{pl} is increased from 0.002 to 0.2. The bandwidth is $0.0604 (2\pi c/a)$ and will cease to change with increasing the value of γ/ω_{pl} . In Fig. 8(b), the relative bandwidth of 1st PBG is also plotted. It can be seen from Fig. 8(b) that the relative bandwidth of such a PBG remains unchanged with changing the value of γ/ω_{pl} . The relative bandwidth is 0.0143. As mentioned above, the damping factor of the ENG material has no effect on the properties of PBG for such 3D PCs. This can be explained by the relationship between ε_p and the damping factor of ENG material γ [40, 56]. We can see from Eq. (1) that the electronic plasma frequency ω_p is much larger than the damping factor of ENG material. The damping factor of ENG material determines only the degree of energy exchange. Thus, the damping factor of ENG material has almost no effects on the real part of ε_p . On the other hand, we can see from Eq. (17) that the damping factor of ENG material obviously has no effect on computing the eigenvalue from a mathematical perspective.

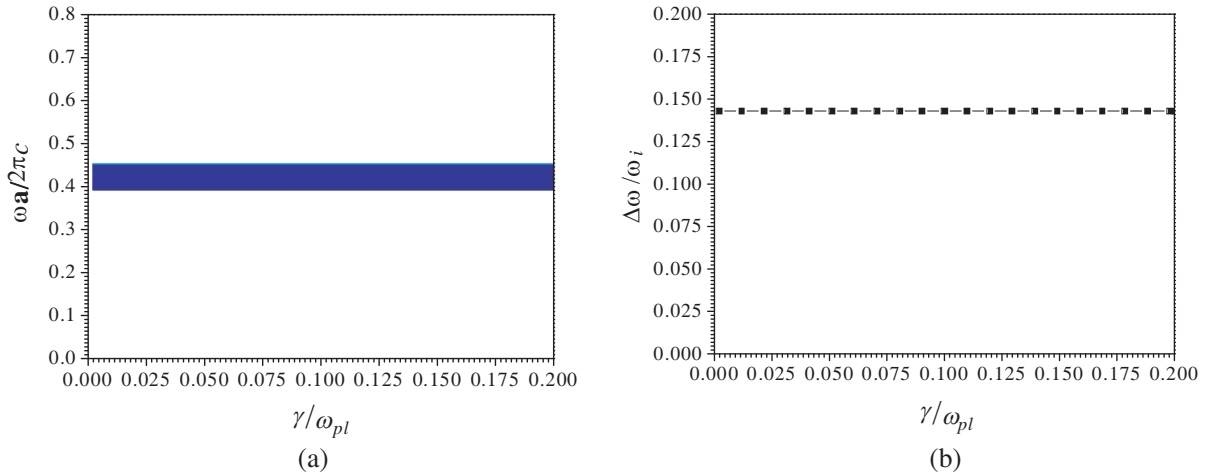


Figure 8. The effects of damping factor γ on the 1st PBG and relative bandwidth for such 3D PCs with $\varepsilon_b = 1$, $\varepsilon_a = 12$, $\omega_p = 0.05\omega_{p0}$ and $R = 0.19a$, respectively. The shaded region indicates the PBG. (a) The PBGs, and (b) relative bandwidths.

On the other hand, such PCs structure can also be realized. The details of realization can be found in the work reported by Garcia-Adeva [46, 47]. Obviously, the models of such 3D PCs as mentioned in our manuscript not only can be realized in the experiment but also can bring the convenience to the theoretical research, because the Fourier form of dielectric constant dyadic of such 3D PCs can be obtained easily. If we want to do the experiment about such 3D PCs, we can also use the layer-by-layer structure to realize the PCs as mentioned in [57]. Obviously, the proposed PCs have an application in realizing the optical devices, such as optical switching, wavelength division multiplexers and filter.

4. CONCLUSIONS

In summary, the properties of PBG for 3D PCs with pyrochlore lattices composed of isotropic positive-index materials and ENG materials which are the dielectric spheres immersed in the uniform ENG materials background are theoretically investigated by the PWE method. The equations for calculating the band structures in the first irreducible Brillouin zone are theoretically deduced. Based on the numerical results, some conclusions can be drawn. Compared to the same structure composed by isotropic dielectrics, the complete PBG and a flatbands region can be obtained as ENG material is introduced. The flatbands are caused by the existence of surface plasmon modes which stem from the coupling effects between the ENG materials. Compared to the conventional topology, such as diamond, fcc, bcc and sc lattices, 3D PCs with pyrochlore arrangement can obtain a larger PBG. The PBG of such 3D PCs can be manipulated by the relative dielectric constant of immersed dielectric, and the general trend for PBG is that relative bandwidth increases with increasing ε_a . The PBG can also be tuned obviously by the dielectric constant of ENG materials. The bandwidth and central frequency of PBG will decrease linearly with increasing ε_b . On the other hand, PBG can be tuned notably by the electronic plasma frequency of ENG material. Increasing the electronic plasma frequency, the bandwidth will increase first and then decrease. The maximum relative bandwidth can be obtained at low- ω_p region. With increasing the filling factor of dielectric spheres, the relative bandwidth and frequency range of PBG will increase first and then decrease. It is also noticed that if filling factor is small enough and close to null, such 3D PCs can be seen as an ENG material block. The flatbands will disappear. The damping factor of ENG material has no effect on the PBG of such PCs. As mentioned above, we can take advantage of the ENG material to form 3D PCs with pyrochlore lattices for obtaining larger complete PBGs as the PCs with low filling factor and dielectric constant.

ACKNOWLEDGMENT

This work was supported by the Natural Natural Science Foundation of China (Grant No. 61307052), the Chinese Specialized Research Fund for the Doctoral Program of Higher Education (Grant No. 20123218110017), the Jiangsu Province Science Foundation (Grant No. BK2011727), in part by the Fundamental Research Funds for the Central Universities (No. NZ2013302), and in part by the Foundation of Aeronautical Science (No. 20121852030).

REFERENCES

1. Yablonovitch, E., "Inhibited spontaneous emission of photons in solid-state physics and electronics," *Phys. Rev. Lett.*, Vol. 58, 2059–2061, 1987.
2. John, S., "Strong localization of photons in certain disordered dielectric superlattices," *Phys. Rev. Lett.*, Vol. 58, 2486–2489, 1987.
3. Rybin, M. V., A. B. Khanikaev, M. Inoue, K. B. Samusev, M. J. Steel, G. Yushin, and M. F. Limonov, "Fano resonance between Mie and Bragg scattering in photonic crystals," *Phys. Rev. Lett.*, Vol. 103, 023901-1–023901-4, 2009.
4. Knight, J. C., J. Broeng, T. A. Birks, and P. S. J. Russell, "Photonic band gap guidance in optical fibers," *Science*, Vol. 284, 1476–1478, 1999.
5. Painter, O., R. K. Lee, A. Scherer, A. Yariv, J. D. O'Brien, P. D. Dapkus, and I. Kim, "Two-dimensional photonic bandgap defect mode laser," *Science*, Vol. 284, 1819–1821, 1999.
6. Miyai, E., M. Okano, M. Mochizuki, and S. Noda, "Analysis of coupling between two-dimensional photonic crystal waveguide and external waveguide," *Appl. Phys. Lett.*, Vol. 81, 3729–3731, 2002.
7. Happ, T. D., M. Kamp, A. Forchel, J. L. Gentner, and L. Goldstein, "Two-dimensional photonic crystal couple-defect laser diode," *Appl. Phys. Lett.*, Vol. 82, 4–6, 2003.
8. Zhang, H. F., M. Li, and S. B. Liu, "Defect mode properties of magnetized plasma photonic crystals," *Acta Phys. Sin.*, Vol. 58, 1071–1076, 2009.

9. Zhang, H. F., S. B. Liu, X. K. Kong, L. Zou, C. Z. Li, and W. S. Qing, "Enhancement of omnidirectional photonic band gaps in one-dimensional dielectric plasma photonic crystals with a matching layer," *Phys. Plasmas*, Vol. 19, 022103, 2012.
10. Zhang, H. F., S. B. Liu, X. K. Kong, B. R. Bian, and Y. Dai, "Omnidirectional photonic band gap enlarged by one-dimensional ternary unmagnetized plasma photonic crystals based on a new Fibonacci quasiperiodic structure," *Phys. Plasmas*, Vol. 19, 22102, 2012.
11. Kwon, S. H., H. Y. Ryu, G. H. Kim, Y. H. Lee, and S. B. Kim, "Photonic bandedge lasers in a two-dimensional square-lattice photonic crystal slab," *Appl. Phys. Lett.*, Vol. 83, 3879–3872, 2002.
12. Monat, C., C. Seassal, X. Letartre, P. Regreny, P. Rojo-Romeo, P. Viktorovitch, M. Le Vassor d'Yerville, D. Cassagne, J. P. Albert, E. Jalaguier, S. Pocas, and B. Aspar, "InP-based two-dimensional photonic crystal on silicon: In-plane Bloch mode laser," *Appl. Phys. Lett.*, Vol. 81, 5102–5104, 2002.
13. Hattori, H. T., I. McKerracher, H. H. Tan, C. Jagadish, R. Michael, and D. L. Rue, "In-plane coupling of light from InP-based photonic crystal band-edge lasers into single-mode waveguides," *IEEE J. Quantum Electron.*, Vol. 43, 279–286, 2007.
14. Zhang, H. Y., Y. P. Zhang, W. H. Liu, Y. Q. Wang, and J. G. Yang, "Zero-averaged refractive-index gaps extension by using photonic heterostructures containing negative-index materials," *Appl. Phys. B*, Vol. 96, 67–70, 2009.
15. Deng, X. H., J. T. Liu, J. H. Huang, L. Zou, and N. H. Liu, "Omnidirectional bandgaps in Fibonacci quasicrystals containing single-negative materials," *J. Phys.: Condens. Matter*, Vol. 22, 055403, 2010.
16. Mocella, V., S. Cabrini, A. S. P. Chang, P. Dardano, L. Moretti, I. Rendina, D. Olynick, B. Harteneck, and S. Dhuey, "Self collimation of light over millimeter-scale distance in a quasi-zero-average-index metamaterial," *Phys. Rev. Lett.*, Vol. 102, 122902, 2009.
17. Kocaman, S., M. S. Aras, P. Hsieh, J. F. McMillan, C. G. Biris, N. C. Panoiu, M. B. Yu, D. L. Kwong, A. Stein, and C. W. Wong, "Zero phase delay in negative-refractive-index photonic crystals superlattices," *Nature Photonics*, Vol. 5, 499–505, 2011.
18. Veselago, V. G., "The electrodynamics of substances with simultaneously negative values of ϵ and μ ," *Sov. Phys. Uspekhi*, Vol. 10, 509–514, 1968.
19. Chen, Y., "Broadband one-dimensional photonic crystal wave plate containing single-negative materials," *Opt. Express*, Vol. 13, 19920–19929, 2010.
20. Chen, Y., "Broadband wave plates: Approach from one-dimensional photonic crystals containing metamaterials," *Phys. Lett. A*, Vol. 375, 1156–1159, 2011.
21. Wang, L. G., H. Chen, and S. Y. Zhu, "Omnidirectional gap and defect mode of one-dimensional photonic crystals with single-negative materials," *Phys. Rev. B*, Vol. 70, 245102-1–245102-6, 2004.
22. Zhang, H. F., S. B. Liu, X. K. Kong, B. R. Bian, and Y. N. Guo, "Dispersion properties of two-dimensional plasma photonic crystals with periodically external magnetic field," *Solid State Commun.*, Vol. 152, 1221–1229, 2012.
23. Zhang, H. F., X. K. Kong, and S. B. Liu, "Analysis of the properties of tunable prohibited band gaps for two-dimensional unmagnetized plasma photonic crystals under TM mode," *Acta Phys. Sin.*, Vol. 60, 055209, 2011.
24. Zhang, H. F., S. B. Liu, and X. K. Kong, "Defect mode properties of two-dimensional unmagnetized plasma photonic crystals with line-defect under transverse magnetic mode," *Acta Phys. Sin.*, Vol. 60, 025215, 2011.
25. Zhang, H. F., S. B. Liu, X. K. Kong, B. R. Bian, and X. Zhao, "Properties of omnidirectional photonic band gaps in fibonacci quasi-periodic one-dimensional superconductor photonic crystals," *Progress In Electromagnetics Research B*, Vol. 40, 415–437, 2012.
26. Zhang, H. F., S. B. Liu, X. K. Kong, B. R. Bian, and Y. Dai, "Omnidirectional photonic band gaps enlarged by Fibonacci quasi-periodic one-dimensional ternary superconductor photonic crystals," *Solid State Commun.*, Vol. 152, 2113–2119, 2012.

27. Zhang, H. F., S. B. Liu, X. K. Kong, B. R. Bian, and B. Ma, "Enhancement of omnidirectional photonic bandgaps in one-dimensional superconductor — Dielectric photonic crystals with a staggered structure," *J. Supercond. Nov. Magn.*, Vol. 26, 77–85, 2013.
28. Kamp, M., T. Happ, S. Mahnkopf, G. Duan, S. Anand, and A. Forchel, "Semiconductor photonic crystals for optoelectronics," *Physica E*, Vol. 21, 802–808, 2004.
29. Moroz, A., "Three-dimensional complete photonic bandgap structures in the visible," *Phys. Rev. Lett.*, Vol. 83, 5274–5277, 1999.
30. Kockaert, P., P. Tassin, I. Veretennicoff, G. V. D. Sande, and M. Tlidi, "Beyond the zero-diffraction regime in optical cavities with a left-handed material," *J. Opt. Soc. Am. B*, Vol. 26, B148–B155, 2009.
31. Krumbholz, N., K. Gerlach, F. Rutz, M. Koch, R. Piesiewicz, T. Kürner, and D. Mittleman, "Omnidirectional terahertz mirrors: A key element for future terahertz communication systems," *Appl. Phys. Lett.*, Vol. 88, 202905, 2006.
32. Kim, K., "Polarization-dependent waveguide coupling utilizing single-negative materials," *IEEE Photonics Technol. Lett.*, Vol. 17, 369–371, 2005.
33. Hsueh, W. J., C. T. Chen, and C. H. Chen, "Omnidirectional band gap in Fibonacci photonic crystals with metamaterials using a band-edge formalism," *Phys. Rev. A*, Vol. 78, 013836, 2008.
34. Wang, Z., C. T. Chan, W. Zhang, N. Ming, and P. Sheng, "Three-dimensional self-assembly of metal nanoparticles: Possible photonic crystal with a complete gap below the plasma frequency," *Phys. Rev. B*, Vol. 64, 113108, 2001.
35. Chan, C. T., W. Y. Zhang, Z. L. Wang, X. Y. Lei, D. Zheng, W. Y. Tam, and P. Sheng, "Photonic band gaps from metallo-dielectric spheres," *Physica B*, Vol. 279, 150–154, 2000.
36. Zhang, W. Y., X. Y. Lei, Z. L. Wang, D. G. Zheng, W. Y. Tam, C. T. Chan, and P. Sheng, "Robust photonic band gap from tunable scatterers," *Phys. Rev. Lett.*, Vol. 84, 2853, 2000.
37. Zhang, H. F., S. B. Liu, and B. X. Li, "The properties of photonic band gaps for three-dimensional tunable photonic crystals with simple-cubic lattices doped by magnetized plasma," *Optics & Laser Technology*, Vol. 50, 93–102, 2013.
38. Zhang, H. F., S. B. Liu, X. K. Kong, and B. R. Bian, "The characteristics of photonic band gaps for three-dimensional unmagnetized dielectric plasma photonic crystals with simple-cubic lattice," *Optic Commun.*, Vol. 288, 82–90, 2013.
39. Zhang, H. F., S. B. Liu, and X. K. Kong, "Analysis of Voigt effects in dispersive properties for tunable three-dimensional face-centered-cubic magnetized plasma photonic crystals," *Journal of Electromagnetic Waves and Applications*, Vol. 27, No. 10, 1276–1292, 2013.
40. Zhang, H. F., S. B. Liu, and X. K. Kong, "Investigating the dispersive properties of the three-dimensional photonic crystals with face-centered-cubic lattices containing epsilon-negative materials," *Applied Physics B*, Vol. 112, 553–563, 2013.
41. Zhang, H. F., S. B. Liu, and X. K. Kong, "Properties of anisotropic photonic band gaps in three-dimensional plasma photonic crystals containing the uniaxial material with different lattices," *Progress In Electromagnetics Research*, Vol. 141, 267–289, 2013.
42. Zhang, H. F., S. B. Liu, and X. K. Kong, "Investigation of Faraday effects in photonic band gap for tunable three-dimensional magnetized plasma photonic crystals containing the anisotropic material in diamond arrangement," *Journal of Electromagnetic Waves and Applications*, Vol. 27, No. 14, 1776–1791, 2013.
43. Zhang, H. F., S. B. Liu, and X. K. Kong, "Dispersion properties of three-dimensional plasma photonic crystals in diamond lattice arrangement," *J. Lightwave Technol.*, Vol. 17, 1694–1702, 2013.
44. Li, Z. Y., J. Wang, and B. Y. Gu, "Creation of partial band gaps in anisotropic photonic-band-gap structures," *Phys. Rev. B*, Vol. 58, 3721–3729, 1998.
45. Malkova, N., S. Kim, T. Dilazaro, and V. Gopalan, "Symmetrical analysis of complex two-dimensional hexagonal photonic crystals," *Phys. Rev. B*, Vol. 67, 125203-1–125203-6, 2003.

46. Garcia-Adeva, A. J., "Band structure of photonic crystals with the symmetry of a pyrochlore lattice," *Phys. Rev. B*, Vol. 73, 073107-1–073107-6, 2006.
47. Garcia-Adeva, A. J., "Band gap atlas for photonic crystals having the symmetry of the kagome and pyrochlore lattices," *New J. Phys.*, Vol. 8, 86-1–86-16, 2006.
48. Garcia-Adeva, A. J., R. Balda, and J. Fernandez, "The density of electromagnetic modes in photonic crystals based on the pyrochlore and kagomé lattices," *Optic. Material*, Vol. 27, 1733–1742, 2005.
49. Lou, M., Q. H. Liu, and Z. Li, "Spectral element method for band structures of three-dimensional anisotropic photonic crystals," *Phys. Rev. E*, Vol. 80, 056702, 2012.
50. Marrone, M., V. F. Rodriguez-Esquerre, and H. E. Hernández-Figueroa, "Novel numerical method for the analysis of 2-D photonic crystals: The cell method," *Opt. Exp.*, Vol. 10, 1299–1304, 2002.
51. Jun, S., Y. S. Cho, and S. Im, "Moving least-square method for the band-structure calculation of 2D photonic crystals," *Opt. Exp.*, Vol. 11, 541–551, 2003.
52. Zhang, H. F., S. B. Liu, X. K. Kong, L. Zhou, C. Z. Li, and B. R. Bian, "Comment on 'Photonic bands in two-dimensional microplasma array. I. Theoretical derivation of band structures of electromagnetic wave'," *J. Appl. Phys.*, Vol. 101, 073304, 2007; *J. Appl. Phys.*, Vol. 110, 026104, 2011.
53. Kuzmiak, V. and A. A. Maradudin, "Photonic band structure of one-and two-dimensional periodic systems with metallic components in the presence of dissipation," *Phys. Rev. B*, Vol. 55, 7427–7444, 1997.
54. Cassagne, D., C. Jouanin, and D. Bertho, "Hexagonal photonic-band-gap structures," *Phys. Rev. B*, Vol. 53, 7134–7142, 1996.
55. Chern, R., C. C. Chang, and C. C. Chang, "Analysis of surface plasmon modes and band structures for plasmonic crystals in one and two dimensions," *Phys. Rev. E*, Vol. 73, 036605-1–036605-16, 2006.
56. Zhang, H. F., S. B. Liu, and X. K. Kong, "Study of the dispersive properties of three-dimensional photonic crystals with diamond lattices containing metamaterials," *Laser Phys.*, Vol. 23, 105815-1–105815-9, 2013.
57. Zhang, H. F., S. B. Liu, and X. K. Kong, "The properties of photonic band gaps for three-dimensional plasma photonic crystals in a diamond structure," *Phys. Plasmas*, Vol. 20, 042110-1–042110-11, 2013.